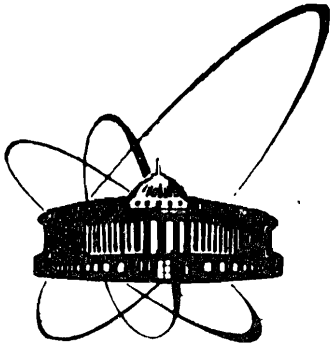

объединенный
институт
ядерных
исследований
дубна

E1-86-129

A-DEPENDENCE OF η-MESON INCLUSIVE PRODUCTION AT 10.5 GeV/c

Submitted to "Nuclear Physics"

1986

G.S.Bitsadze, Yu.A.Budagov, I.E.Chirikov-Zorin,
V.P.Dzhelepov, A.A.Feshchenko, V.B.Flyagin, A.B.Jordanov,
B.Z.Kopeliovich, Yu.F.Lomakin, S.N.Malyukov, N.A.Russakovich,
A.A.Semenov, S.V.Sergeev, J.Spalek, P.Strmen, S.Tokar,
R.V.Tsenov, V.B.Vinogradov
Joint Institute for Nuclear Research, Dubna

S.A.Akimenko, V.I.Beloussov, A.M.Blick, V.I.Kolosov,
B.M.Kut'in, Yu.M.Mel'nik, A.I.Pavlinov, A.S.Solov'ev,
V.V.Tchurakov, A.E.Yakutin
Institute for High Energy Physics, Serpukhov, USSR

V.M.Maniev
Physics Institute of the Azerbaijan Academy of Sciences,
Baku, USSR

I.A.Minashvili
Institute for High Energy Physics of the Tbilisi State
University, Tbilisi, USSR

L.Šandor
Experimental Physics Institute of the Slovak
Academy of Sciences, Košice, Czechoslovakia

Investigations of inclusive production of hadrons with the different quark structure in low-p_T hadron-proton and hadron-nucleus collisions revealed a number of significant points related to the quark-parton structure of hadrons (e.g., see [1,2]). Collisions between hadrons and atomic nuclei seem to be the only way to obtain information on the space-time picture of particle interactions and production. Using the nucleus as a space-time analyser of collision processes, one can get an estimation of such an important dynamic parameter as the hadron formation length [1,3]. Present theoretical concepts essentially differ both in value and interpretation of this parameter.

A standard version of the parton model (see for example [1]) implies a short range character of the interaction in the rapidity scale. After collision of incident hadron and a nucleon, some time must elapse, and only then slow partons appear and wave functions of hadrons, produced in the interaction, are formed. Then the latter became capable to interact with the other nucleons. The corresponding formation length l_p increases with momentum p of hadron produced

$$l_p \simeq p/\mu^2 , \qquad \text{where} \quad \mu^2 \sim 0.5 \ \text{GeV}^2 \ [1].$$

In QCD models [4], on the contrary, the gluon exchange results in a long-range character of the interaction in the rapidity scale. After the primary interaction took place, coloured quarks fly a distance l_f before turning into colourless objects capable to interact. This distance (the quark fragmentation length) equals, for example, $l_f \simeq p/2\varkappa$ in the colour string model [5]. Here $\varkappa$ is the energy per unit of the string length. One can estimate it using the slope of the reggeon trajectories $\alpha'_R \simeq 0.9 \ \text{GeV}^{-2}$

$$\varkappa = 1 / 2\pi\alpha'_R \approx 1 \ \text{GeV/fm} .$$

Comparison of the quark fragmentation length in the colour string model and the hadron formation length in the parton model shows that they are of the same order only in the region of small values of the Feynman's $x_F \lesssim \langle x_F \rangle \approx 0.5$. The cases where one of the hadrons produced carries large part of the initial momentum ($x_F \to 1$) correspond to those rare fluctuations when hadronisation

finishes quickly owing to picking up a slow quark, instead of a gradual decrease of the colour string mass through consequent breaks. This occurs at short distances [6,7]

$$l_f = \frac{p_0}{æ}(1 - x_F), \quad x_F \to 1, \qquad (1)$$

where p_0 is the incident hadron momentum.

This relation reflects the basic assumptions of the model, and it means that the leading quark is slowed down by the coloured string with a force $æ = -dp/dt$ on the path l_f before its fragmentation into a colourless object. The wave function of the observed hadron with the momentum $p = p_0 x_F$ is formed at larger distances of the order of p/μ^2.

Now, if the initial momentum p_0 is large enough, l_f, according to (1), will exceed the nucleus size at some x_F. Then the quark fragmentation and final hadron formation occur behind the nucleus. Because of absorption of the incident hadron, only the front surface of the nucleus works efficiently and the production cross section of the observed hadron $\sigma \sim A^{2/3}$, where A is the nucleus mass number. At $x_F \to 1$ $l_f \to 0$, $\sigma \sim A^{1/3}$ because of absorption of the produced hadron, too. A similar effect was observed [8] at the momentum $p_0 = 100$ GeV/c in inclusive reactions $pPb \to pX$, $\pi^+Pb \to \pi^+X$, but it is difficult to interpret it because of the diffraction dissociation contribution [6].

To clarify this and some other not well understood points in dynamics of inclusive meson production, we have experimentally studied the reactions:

$$h^+ + p \to \eta + X \quad (\eta \to 2\gamma) \qquad (2)$$

$$h^+ + A \to \eta + X \quad (\eta \to 2\gamma) \qquad (3)$$

($h^+ \equiv \pi^+, K^+, p$; $A \equiv D, Li, Be, Al, Cu$) at the momentum 10.5 GeV/c in the beam fragmentation region.

At this initial momentum and at $x_F \sim 0.5$, $æ \sim 1$ GeV/fm the value of l_f is close to dimensions of nuclei with $A \approx 60$.

The η-meson production reactions were chosen for the following reasons:

(i) processes (2) and (3) occur with the change in quantum numbers; therefore there is no diffraction dissociation contribution;

(ii) practically all η-mesons in this energy region are produced in the primary act, i.e., the yield of η-mesons from decays of heavier resonances, which could distort the picture, is negligible;

(iii) reactions (3) are sensitive to the ratio of neutron and proton density on the nucleus surface, that allows its estimation.

At the same time the data on inclusive production of η-mesons at near-by energies are quite scarce. In the bubble chamber experiments [9] only the relevant total cross sections were estimated; for p-Be interactions at 12 GeV/c there are only p_T-distributions in a limited region of small x_F [10]; the paper [11] ($\pi^\pm p$ - interactions at 16 GeV/c) deals with η-meson production only together with charged particles. The recent investigations [12] gave a rather wide set of η-meson yield ratios in different beams, but there was no systematic study of inclusive differential cross sections and their A-dependence.

In this paper we present the new data on the ratios of inclusive differential cross sections $\frac{d\sigma}{dx_F}(\pi^+D \to \eta X) \Big/ \frac{d\sigma}{dx_F}(\pi^+p \to \eta X)$ and $\frac{d\sigma}{dx_F}(\pi^+A \to \eta X) \Big/ \frac{d\sigma}{dx_F}(\pi^+D \to \eta X)$, their A-dependence and interpretation. The results are based on the statistics of $\approx 5 \cdot 10^4$ detected $\eta \to 2\gamma$ decays. Earlier we have published [13] data on relative yields of η-mesons in π^+D- and K^+D-interactions, using part of the same statistics.

1. Measurements and Data Analysis

A part of HYPERON-spectrometer [14] detectors (Fig. 1a) was used for measurements. Gamma-quanta from decays of η-mesons produced in interactions of the beam particles in the target T were detected in a Cherenkov 62-channel shower hodoscope detector SHD with an active converter AC (Fig. 1b). Elements of the SHD (10x10x35 cm^3) and AC (6x10x85 cm^3) are made of lead glass TFI-000 (2.5 cm radiation length). Proportional chambers PC and a scintillation hodoscope H were used for reconstruction of secondary charged particle tracks.

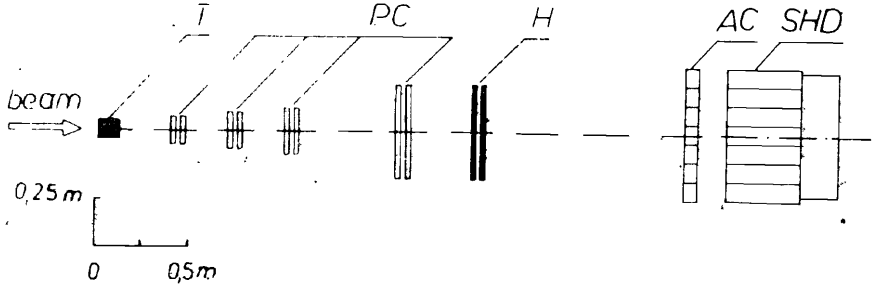

Fig. 1a. Experimental facility.

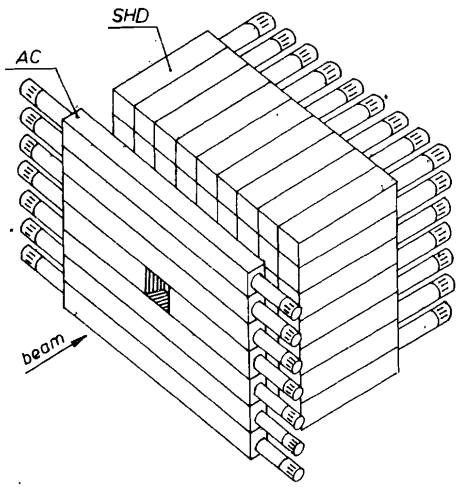

Fig. 1b. Shower hodoscopic detector with active converter.

A detailed description of the design and basic characteristics of the SHD and AC, calibration and monitoring procedures and trigger logic are given elsewhere /13,15/.

During the experiment $3.4 \cdot 10^9$ π^+-mesons passed through the facility. Table 1 lists parameters of the targets used and corresponding π^+-monitors.

In the data analysis only the events with $\geq 2\gamma$'s were considered. The average γ-multiplicity in the selected events was 2.13. The effective mass $M_{\gamma\gamma}$, the transversal momentum p_T and the Feynman's variable $x_F = p_\parallel^*/(p_\parallel^*)_{max}$ were calculated for each $\gamma\gamma$-pair. The value of $(p_\parallel^*)_{max}$ was determined from the charge exchange reaction $\pi^+ n \to \eta p$. When calculating kinematic parameters, the interaction point was found as the intersection of the beam track with the secondary charged particles tracks. If the latter were not detected, the middle of the target was regarded as the interaction point.

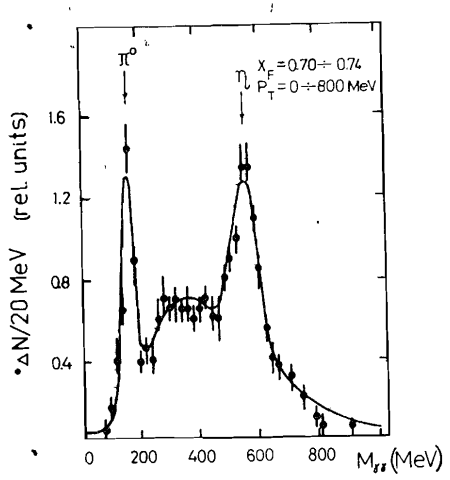

Fig. 2. An example of events distribution over the invariant mass of $\gamma\gamma$-pairs in the reaction $\pi^+ D \to \gamma\gamma + X$. Detection of $\gamma\gamma$-pairs with a mass < 400 MeV/c^2 is suppressed by special trigger conditions applied /13,15/.

After normalisation to the monitor of π^+-mesons and "empty/no target" background subtraction the number of events ($\gamma\gamma$-combinations) in

Table 1. Targets used, their characteristics, monitor of π^+-mesons

Target	Mass number A	Length λ (cm)	λ / λ_0	λ / X_0	π^+-monitors x 10^6
H	1.01	27.5	0.038	0.032	715
D	2.01	27.5	0.083	0.036	562
Li	6.94	20.0	0.146	0.129	114
Be	9.01	2.5	0.061	0.071	125
		5.0	0.123	0.142	87
		10.0	0.246	0.283	53
Al	26.98	1.75	0.044	0.197	149
		3.5	0.089	0.393	112
		7.0	0.178	0.787	61
Cu	63.54	0.69	0.046	0.483	167
		1.38	0.092	0.965	114
		2.04	0.135	1.43	127
		2.74	0.182	1.92	52
Empty cryogenic target					719
No target					273

λ_0 - nuclear interaction length

X_0 - radiation length

each (x_F, p_T)-interval was corrected for the detection efficiency $\varepsilon_{\gamma\gamma}(x_F, p_T)$ calculated by the Monte-Carlo method taking into account the geometrical acceptance, trigger logic and the event reconstruction efficiency. Then $M_{\gamma\gamma}$-distributions, integrated over the $p_T = 0 \div 0.8$ GeV/c were obtained for each x_F-interval. A typical example of such distribution is shown in Fig. 2.

The η-mesons number in each x_F-interval for each target (or for each target thickness if there were several of them) was determined by fitting an experimental $M_{\gamma\gamma}$-spectra to the function:

$$F(M_{\gamma\gamma}) = N^{\pi^0} \cdot G^{\pi^0}(M_{\gamma\gamma}) + N^{\eta} \cdot G^{\eta}(M_{\gamma\gamma}) + N^{bg} \cdot BG(M_{\gamma\gamma}),$$

where $G^{\pi^0,\eta}(M_{\gamma\gamma})$ are Gauss distributions for peaks from π^0- and

η-meson decays, BG ($M_{\gamma\gamma}$) is the gamma-distribution describing the non-resonant background. In a given x_F-interval the fit* was carried out simultaneously for all 13 $M_{\gamma\gamma}$-distributions (accordingly to the number of targets used, see Table 1). Parameters in $G^{\pi^0,\eta}$ and BG were not fixed but the same for all 13 spectra fitted.

Contributions from π^0- and η-peaks and a contribution of the background had the form:

$$N_{A,i}^{\pi^0,\eta,bg} = a_A^{\pi^0,\eta,bg} \cdot \lambda_i \exp(-\beta \lambda_i / X_{0,A}) ,$$

where A ≡ H, D, Li, Be, Al, Cu and i corresponds to a measurement with a target thickness λ_i. $a_A^{\pi^0,\eta,bg}$ are free parameters. $X_{0,A}$ is the radiation length of the material A. The exponential factor takes into account γ-losses in the target. It was significant only for Al- and Cu-targets. The parameter β was determined from the normalized numbers of events in $M_{\gamma\gamma}$-histograms for targets of different thicknesses (see Table 1). As one could expect, it did not depend on A. In addition, no x_F-dependence was found. Thus, β was fixed for all targets and x_F-intervals on its average value, $\beta = 0.35$.

As a result of the fit, values of free parameters $a_A^{\pi^0,\eta,bg}$ were obtained and the η-meson production cross section was computed as:

$$\frac{d\sigma}{dx_F}(\pi^+ A \to \eta X) = \text{const} \cdot \frac{A}{\rho_A} a_A^{\eta} ,$$

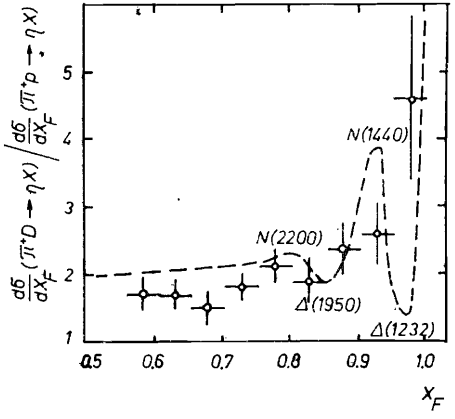

where ρ_A is the density, A is the mass number. The data for ratios

Fig. 3. Ratio of differential cross sections for production of η-mesons on a deuteron and a proton. The dashed curve is the result of calculations (Section 2.1).

* By means of the computer code MINUIT /16/.

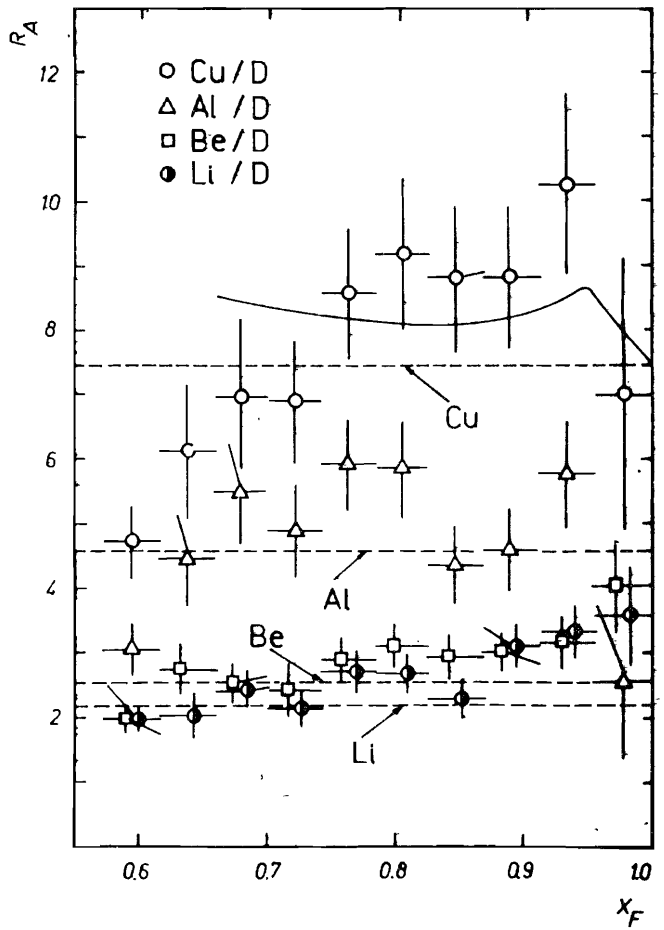

Fig. 4a. Ratios of differential cross sections.

$R_A = \frac{d\sigma}{dx_F}(\pi^+ A \to \eta X) \Big/ \frac{d\sigma}{dx_F}(\pi^+ D \to \eta X)$, where A ≡ Li, Be, Al, Cu.

The dashed straight lines show calculations in the Glauber's approach. The solid curve shows the calculation with allowance for rescatterings. The maximum at $x_F \simeq 0.95$ is due to the contribution of the charge exchange reaction $\pi^+ n \to \eta p$.

Table 2. Ratios of inclusive differential cross sections for η-meson production and the parameter α

x_F-interval	$R_{D/p}$	$R_A(x_F)$				$\alpha(x_F)$
		Li/D	Be/D	Al/D	Cu/D	
0.57-0.62	1.74±0.42	2.01±0.21	2.00±0.20	3.08±0.38	4.76±0.55	0.403±0.049
0.62-0.66	1.91±0.38	2.06±0.36	2.75±0.39	4.44±0.69	6.15±1.00	0.412±0.057
0.66-0.70	1.52±0.24	2.44±0.28	2.54±0.34	5.49±0.78	7.01±1.18	0.521±0.065
0.70-0.74	1.87±0.19	2.16±0.28	2.43±0.35	4.93±0.70	6.93±0.93	0.540±0.053
0.74-0.78	2.20±0.26	2.72±0.29	2.92±0.31	5.96±0.70	8.59±0.98	0.541±0.046
0.78-0.83	1.94±0.28	2.71±0.30	3.12±0.32	5.91±0.71	9.21±1.16	0.554±0.052
0.83±0.87	2.37±0.38	2.30±0.29	2.92±0.30	4.37±0.60	8.84±1.11	0.554±0.056
0.87-0.91	2.64±0.41	3.17±0.32	2.99±0.29	4.64±0.63	8.86±1.09	0.468±0.054
0.91-0.96	5.68±1.85	3.35±0.40	3.21±0.36	5.80±0.80	10.3 ±1.39	0.491±0.049
0.96-1.00	23.1 ±52.4	3.59±0.72	4.08±0.71	2.58±1.16	7.02±2.08	

$$R_{D/p}(x_F) = \frac{d\sigma}{dx_F}(\pi^+ D \to \eta X) \Big/ \frac{d\sigma}{dx_F}(\pi^+ p \to \eta X), \qquad (4)$$

$(p_T \leq 0.8$ GeV/c)

and

$$R_A(x_F) = \frac{d\sigma}{dx_F}(\pi^+ A \to \eta X) \Big/ \frac{d\sigma}{dx_F}(\pi^+ D \to \eta X), \qquad (5)$$

where A ≡ Li, Be, Al, Cu, are given in Table 2 and in Fig. 3 and 4. We give ratios of cross sections on nuclei to those on deuterium (not on hydrogen) because of approximately equal proportions of ptotons and neutrons in deuterium and nuclei.

The indicated errors were calculated from the errors of parameters a_A^η estimated in the fitting procedure /16/.

Ratios R_A were parametrised (χ^2/NDF = 0.9 in average) by the relation

$$R_A(x_F) \sim A^{\alpha(x_F)} \qquad (6)$$

The $\alpha(x_F)$ values are given in the last column of Table 2 and in Fig. 5.

2. Discussion

Further we will restrict ourselves to the following questions:

(i) why the ratio (4) shows a strong x_F-dependence at $x_F \geq 0.9$;

(ii) what can be said about validity of relation (1) and the value of the parameter æ ;

(iii) what is the explanation for increase in ratios (5) when x_F grows.

Fig. 4b. Results of calculations of $R_{Cu}(x_F)$, described in sections 2.2 and 2.3.

2.1. Ratio $R_{D/p}$

Obviously, the cross section of the reaction $\pi^+N \to \eta X$ is insensitive to the type of the target nucleon at large missing masses M_x, and $R_{D/p}(x_F) \to 2$. In the region of nucleon resonances excitation, on the contrary, the cross sections on the neutron and proton differ significantly. At the limit $x_F \to 1$, for instance, charge exchange reaction on the proton is forbidden by the charge conservation law. The cross section for the process

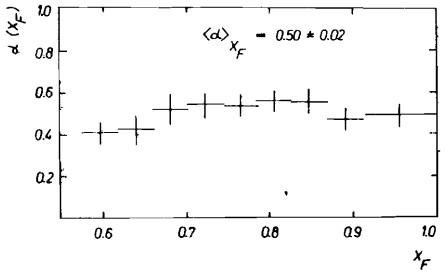

Fig. 5. $\alpha(x_F)$ in the parametrisation $R_A(x_F) \sim A^{\alpha(x_F)}$.

$\pi^+N \to \eta X$ at large x_F can be described by a two-reggeon graph (Fig. 6), corresponding to the A_2-meson exchange. Then, one can present the ratio $R_{D/p}$, ignoring the inelastic shielding in the deuteron, in the form:

$$R_{D/p}(x_F) = \frac{\sigma_{tot}^{A_2 n}(s')}{\sigma_{tot}^{A_2 p}(s')} + 1 , \qquad (7)$$

where $s' = s(1-x_F)$, and s is the c.m. total energy squared.

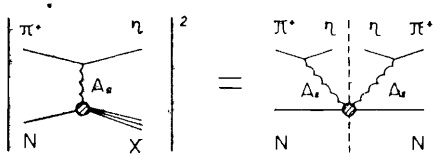

Fig. 6. Basic two-reggeon graph for description of the inclusive process $\pi^+N \to \eta X$ at $x_F \to 1$.

Since there are no data on $\sigma_{tot}^{A_2 N}$, the x_F-dependence of the ratio (7) can be illustrated with $\sigma_{tot}^{\pi^+}$ instead of A_2, because they have similar quantum numbers. The results of this estimation using the data on $\sigma_{tot}^{\pi^+ p}$ and $\sigma_{tot}^{\pi^+ n}$ are shown with the dashed line in Fig. 3. The observed increase at $x_F > 0.9$ is mostly due to excitation of the N(1400)-resonance.

2.2. Fragmentation Length l_f and Parameter æ

In spite of proton-neutron cross section difference, since the number of neutrons and protons in nuclei is approximately the same,

one can analyse nucleus-to-deuterium ratio (5) in terms of averaged cross section on the nucleon both for total and differential cross sections. Then

$$\frac{d\sigma}{dx_F}(\pi^+A \to \eta X) = \frac{d\sigma}{dx_F}(\pi^+N \to \eta X) \cdot A_{eff}(x_F) , \qquad (8)$$

where the effective number of nucleons in a nucleus depends on the fragmentation length l_f :

$$A_{eff}(x_F) = \int d^2b \int_{-\infty}^{\infty} dz\, \rho(\vec{b},z) \left[1 - \frac{\sigma_{inel}^{\pi^+N}}{A} \int_{-\infty}^{z} dz'\rho(\vec{b},z') - \frac{\sigma_{inel}^{\eta N}}{A} \int_{z+l_f(x_F)}^{\infty} dz'\rho(\vec{b},z') \right]^{A-1} . \qquad (9)$$

Here $\vec{b}$ is the impact parameter, z is the coordinate along the momentum of the incident π^+-meson; $\sigma_{inel}^{\eta N} \approx \sigma_{inel}^{\pi^+N} \approx 20$ mb are the total inelastic cross sections for interactions of η - and π^+-mesons with a nucleon. The nuclear density $\rho(\vec{b},z)$ is chosen in Woods-Saxon's form. Parameters of $\rho(\vec{b},z)$ for various nuclei are given in the paper /17/. At $l_f \to 0$ expression (9) turns into the usual Glauber's formula for the effective number of nucleons and $R_A(x_F) = \text{const}$. Fig. 4b shows the results of calculations for $R_A(x_F)$ at A = 64 (a copper target), where the strongest x_F-dependence is expected. The results are represented for several values of æ (æ $\to \infty$ corresponds to Glauber's case). One can see that at æ $\geq$ 3 GeV/fm for $x_F \geq 0.6$ (the kinematic region covered) calculated R_{Cu} is practically independent of x_F. This reflects the fact that for æ $\geq$ 3 GeV/fm and $x_F \geq 0.6$ $l_f \leq 1.4$ fm and it is smaller than the mean distance between the nucleons. As the data for R_{Cu} does not reveal any decreasing as x_F grows, one can conclude that the quark fragmentation length does not manifest itself at our energy, i.e., æ $\geq$ 3 GeV/fm.

This result seems to be important, since the obtained lower limit for æ is noticeably higher than the value æ = 1 GeV/fm for the static string.* The difference probably reflects the fact that the coloured objects are slowed down not only by the string tension, but also by the gluon bremsstrahlung when colour is exchanged. The last leads to an effective increase in æ.

---

* The confidence level P_{χ^2} (æ = 3 GeV/fm) $\approx$ 8%, while P_{χ^2} (æ = = 1 GeV/fm) $\approx$ 0.01%.

We note that this lower limit agrees with the value $\varkappa \approx 3$ GeV/fm obtained from the data on large-p_T hadron pair production and J/ψ hadroproduction on nuclei [7,18].

As it was shown, the leading quark fragmentation length is small and one can expect that ratios $R_A(x_F)$ should be constant in the x_F-region considered and equal to $A_{eff}/2$, where A_{eff} is determined by formula (9) with $l_f = 0$ (horizontal dashed lines in Fig. 4a). The data are seen to disagree with this simple description.

We performed calculations, based on the triple-reggeon approach, for taking into account the corrections to the ratios R_A, arising from the possible rescattering of the particle produced:

$$\pi^+N \longrightarrow \eta X \hookrightarrow \eta N \longrightarrow \eta X,$$
$$\pi^+N \longrightarrow \pi^+ X \hookrightarrow \pi^+ N \longrightarrow \eta X.$$

The result for R_{Cu} is shown in Fig. 4a with solid line. The agreement with the data is rather poor, too.

2.3. Why do ratios $R_A(x_F)$ grow up as x_F increases

In the previous paragraph we have ignored cross section difference for the η-meson production on the proton and neutron and have used the averaged cross section. On the other hand, our data (see Fig. 3 and discussion in Section 2.1) show considerable difference between those cross sections at large x_F.

The fact that the value of α in parametrisation (6) differs much from unity ($\langle\alpha\rangle = 0.50 \pm 0.02$, Fig. 5) indicates that the process $\pi^+A \to \eta X$ takes place on nucleons in the nuclear periphery, where some abundance of neutrons over protons is expected. The problem of neutron "halo" has been under discussion for a long time (see the review [19]). According to some estimations [19], the neutron-to-proton surface density ratio

$$H = \rho_n / \rho_p \qquad (10)$$

called the neutron halo factor, is quite large for neutron-abundant nuclei: $H \approx 2 \div 5$.

To estimate influence of the halo, we write down the cross section for the process $\pi^+A \to \eta X$ in the form:

$$\frac{d\sigma}{dx_F}(\pi^+A \to \eta X) = \int d^2b \int_{-\infty}^{\infty} dz \left[\frac{d\sigma}{dx_F}(\pi^+n \to \eta X)\rho_n(\vec{b},z) + \frac{d\sigma}{dx_F}(\pi^+p \to \eta X)\rho_p(\vec{b},z) \right] \left[1 - \frac{\sigma_{inel}^{\pi N}}{A} T(\vec{b}) \right]^{A-1}, \qquad (11)$$

where $T(\vec{b})$ is the nucleus profile function, and the relevant densities are normalised in a usual way:

$$\int d^3r \rho_n(\vec{r}) = A - Z,$$
$$\int d^3r \rho_p(\vec{r}) = Z,$$

where Z is the nuclear charge. From (11) we get for ratios (5) with allowance for (10) and (4)

$$R_A(x_F) = \frac{H}{H+1}\left(1 - \frac{H-1}{H\, R_{D/p}(x_F)}\right) \cdot A_{eff}. \qquad (12)$$

To calculate $R_A(x_F)$ according to (12), we used our data on $R_{D/p}(x_F)$ and choose $H=4$. The result is shown in Fig. 4b. The agreement with the data seems quite satisfactory in the whole x_F-region covered.

There is at least one more possible reason for the growing $R_A(x_F)$ at $x_F \to 1$. In the given considerations we did not take into account corrections for inelastic shielding which makes the nucleus more transparent for hadrons. Those corrections are usually small ($\lesssim 10\%$) in total cross sections, but allowance for them can appreciably decrease the probability of the fast hadron's absorption in the nuclear matter [6]. This effect will be considered in a separate paper.

3. Conclusions

(i) The lower limit for the value of the effective coefficient of the coloured triplet string tension $\varkappa \geqslant 3$ GeV/fm is obtained. This value exceeds the estimation for the static string, but agrees with a few relevant estimations [7,18]. Leading quark fragmentation length at an energy of about 10 GeV is small, and hadron-nucleus interactions can be described in Glauber's approach.

(ii) Increase of $R_A(x_F)$ at $x_F > 0.5$ can be obtained if one assumes a considerable neutron abundance on the nuclear periphery with the halo factor $H \approx 4$.

Finally, the authors express their gratitude to Yu.D.Prokoshkin for support and attention, to N.P.Moshkov, S.P.Zhunin, P.V.Simonov and M.V.Tikhonov for great assistance in producing detectors and assembling the whole facility.

References

1. Nikolaev N.N. Usp.Fiz.Nauk,1981, 134, p. 369
2. Fialkowski K., Kittel W. Rept.Prog.Phys., 1983, 46, p. 1283
3. Kancheli O. JETP Letters,1973, 18, p. 469

4. Low F. Phys.Rev.D, 1975, 12, p. 163
5. Casher A. et al. Phys.Rev.D, 1979, 20, p. 179
6. Kopeliovich B.Z., Lapidus L.I. In: Proc.of the 6-th Balaton Conf.on Nucl.Phys., Balatonfured, 1983, p. 73
Kopeliovich B.Z. In: Proceedings of the 19-th LNPI Winter School of Physics, Leningrad, 1984, p. 169
7. Kopeliovich B.Z., Niedermayer F. Yad.Fiz., 1985, 42, p. 797
8. Barton D. et al. Phys.Rev.D, 1983, 27, p. 2580
9. Jaeger K. et al. Phys.Rev.D, 1975, 11, p. 1756
Borg A.C. et al. Nucl.Phys.B, 1976, 106, p. 430
10. Kanzaki O. et al. J.Phys.Soc.Japan,1981, 50, p. 3849
11. Bartke J. et al. Nucl.Phys.B, 1977, 106, p. 360
12. Akimenko S.A. et al. Yad.Fiz., 1983, 38, p. 1212
Akimenko S.A. et al. Yad.Fiz., 1984, 39, p. 649
13. Akimenko S.A. et al. IHEP Preprint 85-93, Serpukhov, 1985
14. Antjukhov V.A. et al. Prib.i Tekhn.Eksperim.,1985, 5, p. 35
15. Bitsadze G.S. et al. JINR Preprint,E1-85-610, Dubna, 1985
16. James F., Roos M. Comput.Phys.Comm., 1975, 10, p. 343
17. Murthy P. et al. Nucl.Phys.B, 1975, 92, p. 269
18. Kopeliovich B.Z., Niedermayer F. JINR Rept., E2-84-834, Dubna, 1984
19. Vorob'ev A.A. In: Proceedings of the 10-th LNPI Winter School of Physics, Leningrad, 1975, p. 5.

Received by Publishing Department
on March 5, 1986.